https://doi.org/10.5194/acp-2020-681
Preprint. Discussion started: 12 August 2020

Atmospheric Chemistry and Physics
Discussions

A measurement and model study on ozone characteristics in marine air at a remote island station and its interaction with urban ozone air quality in Shanghai, China

Yixuan Gu[a,b], Fengxia Yan[c], Jianming Xu[a,b,*], Yuanhao Qu[a,b], Wei Gao[a,b]

[a]Shanghai Typhoon Institute, Shanghai Meteorological Service, Shanghai 200030, China

[b]Shanghai Key Laboratory of Meteorology and Health, Shanghai Meteorological Service, Shanghai 200030, China

[c]Meteorological Center of Traffic Management of East China, Shanghai 2000135, China

Corresponding to: Dr. Jianming Xu (metxujm@163.com)

Keywords: Ozone in oceanic air, Urban Plume, Coastal city air pollution, Shanghai

https://doi.org/10.5194/acp-2020-681
Preprint. Discussion started: 12 August 2020

Abstract

To understand the characteristics and changes of baseline ozone (O_3) in oceanic air in East China, a six-year measurement of O_3 concentration was conducted from January 1 2012 to September 15 2017 at a remote offshore station located on the Sheshan Island (SSI) near the megacity of Shanghai. The observed monthly mean O_3 concentrations at SSI ranged from 33.4 to 61.4 ppbv during the study period, which were about 80% and 12% higher, respectively than those measured at downtown and rural sites in Shanghai. Compared to the remarkable O_3 increases observed at urban and rural sites in Shanghai, observed O_3 concentrations at SSI exhibited statistically insignificant increasing changes (1.12 ppbv yr^{-1}, $\alpha>0.10$) during the observation period, suggesting less impacts of anthropogenic emissions on O_3 levels in oceanic air. In addition, an insignificant decreasing change (-0.72 ppbv yr^{-1}, $\alpha>0.10$) was detected in O_3 concentrations at SSI in September and October when the influence of regional transport was minimum throughout the year, providing a good proxy to study the baseline oxidation capacity of the oceanic atmosphere. City plumes from Shanghai usually carried higher levels of NO_x, resulting in decreased O_3 concentrations at SSI during southwesterly and westerly winds. However, In MAM (March–May) and JJA (June–August), due to the enhanced oxidation of oxygenated volatile organic compounds, O_3 could be continuously produced during daytime in aged city plumes, resulting in elevated O_3 concentrations transported to SSI. The impacts of the offshore O_3 on O_3 levels in Shanghai are quantified during an easterly wind dominant episode (September 1–30, 2014) using the WRF-Chem model. Sensitivity results suggest that O_3 in the oceanic air inflows can lead to 20–30% increases in urban

O_3 concentrations, which should be crucially considered in dealing with urban O_3 pollution in large coastal cities like Shanghai.

1 Introduction

Ground-level ozone (O_3) is a harmful photochemical oxidant detrimental to air quality, human health and land ecosystems (Yue and Unger 2014; Monks et al., 2015; Li et al., 2019a). High ambient O_3 has been proved to increase the risks of respiratory and cardiovascular mortality (Goodman et al., 2015) and enhance the greenhouse effect (IPCC, 2013). In recent years, O_3 pollution has drawn increasing attention in China, since O_3 pollution is getting worse in spite of the implementation of Chinese Clean Air Action Plan. In contrast to the 28-40% decreases in $PM_{2.5}$ (fine particulate matter; diameter ≤ 2.5 μm) levels, the observed daily maximum 8-h average (MDA8) O_3 concentrations show increasing rates of 1–3 ppb yr^{-1} in summer in megacities over eastern China during 2013–2017 (Li et al., 2019b). To address the underlying causes of the increasing O_3 pollution has become an urgent issue that triggers lots of discussions based on observational and model studies worldwide.

Observational and model studies indicated that the elevated O_3 levels in urban and rural areas in eastern China were strongly related to the changes in anthropogenic emissions of O_3 precursors (Ma et al., 2016; Lu et al., 2018; Li et al., 2019b; Gu et al., 2020). Since the O_3 formation was reported to be under volatile organic compound (VOC) limited regime in most Chinese megacities (e.g. Beijing, Shanghai, and Guangzhou), the sharp decreases in nitrogen oxides (NO_x=NO+NO_2) emissions combined with slight increases in VOC levels were suggested to be main causes of the observed enhancement of O_3 concentrations in East China (Gao et al., 2017; Xu et al., 2019). In remote areas, changes of baseline O_3 also exhibit sensitive responses to human activities (Vingarzan, 2004; Meng et al., 2009; Wang et al., 2009; Lin et al., 2015). Based on 14-year observations, Wang et al. (2009) pointed out that enhanced pollution flow from the upwind coastal regions contributed to most of the observed increases in O_3 concentrations during 1994–2007. And the increase in background O_3 likely made a strong contribution (81%) to the increasing rate of O_3 in urban Hong Kong. To understand the background O_3 changes and its response to human activities are thus necessary in developing long-term strategies to mitigate local O_3 pollution. However, compared to the intensive field studies in polluted cities and surrounding rural regions, continuous observations of O_3 at representative background sites are relatively limited in China (Wang et al., 2017).

To better understand the characteristics of the background O_3 changes in mainland China, the China Meteorological Administration (CMA) started to conduct continuous measurements of surface O_3 at several regional background stations (e.g. Shangdianzi, Linan, and Longfengshan) since 2005. Over 10-year records from the three sites and Waliguan, a baseline Global Atmospheric Watch (GAW) station in Tibetan Plateau region, exhibited different increases in background continental O_3 concentrations especially during daytime in China (Lin et al., 2008; Xu et al., 2008; Meng et al., 2009; Ma et al., 2016; Xu et al., 2016). The detected positive trends of surface O_3 were in a range of 0.24–1.13 ppbv yr^{-1}, suggesting enhanced atmospheric oxidation capacity response to the rapid development of urbanization and industrialization in the past decades. In addition to the changes in background O_3 in terrestrial stations mentioned above, the characteristics of baseline O_3 at remote marine sites are also important. It is because that large amounts of O_3 pollution events occurred in coastal urban agglomerations in East China (Lu et al.,

https://doi.org/10.5194/acp-2020-681
Preprint. Discussion started: 12 August 2020

2018; Li et al., 2019a, b), affected by both city plumes and oceanic air inflows (Tie et al., 2009; Shan et al., 2016). For example, model work of Tie et al. (2009) suggested that sea air masses carried by oceanic inshore air flows aggravated urban O_3 pollution in Shanghai under convergence conditions. Understanding the O_3 characteristics in offshore oceanic regions is therefore an important prerequisite for understanding the land-sea O_3 interactions and its impacts on O_3 pollution in coastal cities. However, to our knowledge, studies on the characteristics and changes of O_3 in marine air are quite limited in mainland China since it is very difficult to conduct systematic and continuous observations under remote oceanic air conditions.

In this report, we present the first relatively long and continuous measurements of O_3 conducted on a remote offshore island (Sheshan Island, SSI) from Jan 2012 to Sep 2017 in eastern China. The SSI is located at the confluence of the Yellow Sea and the East China Sea, covering about 0.4 square kilometers area. Since there are no inhabitants in the island, the observed O_3 is seldom affected by local anthropogenic emissions. The collected O_3 data are used to understand the magnitudes and variabilities of O_3 in the offshore regions and their impacts on the O_3 concentrations in coastal city areas. First shown are the general impacts of regional transport on the remote atmosphere over the SSI region. Then the diurnal patterns of O_3 at SSI are investigated by comparing them with those observed at a downtown site (XJH) in Shanghai. Multi-year changes of O_3 concentrations at SSI are analyzed to examine the overall changes of baseline O_3 in marine air and possible causes. Also analyzed are the impacts of urban plumes on O_3 levels in oceanic air in offshore regions. At last, the influence of O_3 carried by oceanic air inflows on urban O_3 air quality in Shanghai is assessed using the Weather Research and Forecasting model coupled with Chemistry (WRF-Chem).

2 Material and methods

2.1 The SSI site and ozone observations

To investigate the characteristics and variabilities of O_3 in marine air and their interactions with urban air quality in coastal areas, ground O_3 concentrations were continuously measured at SSI site (31.4˚N, 122.3˚E, 73.5 m a.s.l.), which is approximately 75 kilometers away from the east edge of Shanghai city. Figure 1 shows the location of SSI and the surrounding environment. As mentioned in Sect. 1, there is no resident and tourist on the island. The observed O_3 at SSI site can represent the background O_3 conditions in oceanic air which are seldom contaminated by anthropogenic emissions. Hourly O_3 data was collected during January 1 2012 to September 15 2017, with a capture rate of 89.7%. O_3 was measured using an analyzer from Ecotech, Australia (Model EC9810), which combined microprocessor control with ultraviolet photometry. The instrument met the technical specifications for United States Environmental Protection Agency, with a quality control check every 3 days, filer replaced every 2 weeks and calibration every month.

2.2 Observational data at urban and rural sites in Shanghai

To better understand the characteristics of the offshore O_3 in oceanic air at SSI, O_3 observations obtained from a downtown site, Xujiahui (XJH) are used for comparisons. The XJH site is located at downtown Shanghai, approximately 80 km west from the SSI. In addition, since measurements of NO_x, carbon monoxide (CO) and meteorological parameters (e.g. wind direction and wind speed) were unavailable at SSI, observations obtained at an adjacent site, Dongtan (DT), are substituted for the investigation. The DT site was set up in a national nature reserve near the coast of Shanghai, where the observed pollutant levels have been reported to well reflect the impacts of pollution transport during the MIRAGE-Shanghai (Megacities Impact on Regional and Global Environment at Shanghai) field campaign (Tie et al., 2013). Similar to SSI, the DT site is also little affected by human activities. The obtained observations of meteorology and pollutants are therefore applied for analyzing the impacts of regional transport on observed O_3 concentrations at SSI. NO_x concentrations were measured with a chemiluminescent trace level analyzer (TEI; Model 42iTL), with detection limit of 0.025 ppb. CO concentrations were measured by the Model 48iTL Enhanced CO analyzer, based on gas filter correlation technology. The wind speed and wind direction were measured by using a DZZ4 Automatic Weather Station certificated by the China Meteorological Administration. The geographical locations and surrounding environment of XJH, DT, and SSI are displayed in Fig. 1.

2.3 The WRF-Chem model

We simulate O_3 using the regional chemical transport model WRF-Chem (version 3.8, https://www2.acom.ucar.edu/wrf-chem), collaboratively developed through efforts of several institutes, such as the National Center for Atmospheric Research (NCAR) and the National Oceanic and Atmospheric Administration (the National Centers for Environmental Prediction (NCEP). The model includes on-line calculation of meteorological parameters, transport, mixing, emission, and chemical transformation of trace gases and aerosols (Grell et al., 2005). The Regional Acid Deposition Model version 2 (RADM2, Stockwell et al., 1990) gas-phase chemical mechanism is used for the O_3 formation chemistry. Photolysis rates are calculated by using the fast radiation transfer module (FTUV) followed those in Madronich and Flocke (1999) and Tie et al. (2003). ISORROPIA II secondary inorganic (Fountoukis and Nenes, 2007) and the Secondary ORGanic Aerosol Model (SORGAM) (Schell et al., 2001) schemes are used for aerosol chemistry. Dry deposition follows the standard resistance-in-series model of Wesely (1989). The major physical processes employed in the model follow the Lin microphysics scheme (Lin et al., 1983), the Yonsei University (YSU) planetary boundary layer (PBL) scheme (Hong and Lim, 2006), the Noah Land surface model (Chen and Dudhia, 2001), and the long-wave radiation parameterization (Dudhia, 1989).

The model used in this study has a horizontal resolution of 6km×6km, including 150 un-staggered grids in west-east, 150 un-staggered grids in south-north, and 35 vertical layers extending from the surface to 50 hPa. The domain encompasses Shanghai and surrounding region, centered at 31.3°N, 121.4°E. The NCEP FNL (Final) Operational Global Analysis data are used for meteorological initial and boundary conditions, with lateral meteorological boundary updated every 6 h. Basic chemical lateral boundary conditions are constrained by a global chemical transport model (MOZART-4, Model for OZone And Related chemical Tracers, version 4) (Tie et al., 2001; Emmons et al., 2010). Anthropogenic emissions are derived from the Multi-resolution Emission Inventory for China (MEIC inventory, http://www.meicmodel.org/; Li et al., 2014) for year 2010. Biogenic emissions are calculated online using model of emissions of gases and aerosols from nature (MEGAN2, Guenther et al., 2006).

https://doi.org/10.5194/acp-2020-681
Preprint. Discussion started: 12 August 2020

2.4 Methods for assessing the trend of ozone

The daily mean O_3 concentrations are used to examine the overall changes in O_3 concentrations during the period 2012–2017, including all time of day with qualified measurements. The trends are assessed using two nonparametric methods, which are commonly used to detect trends of non-normally distributed data with seasonality (Xu et al., 2016).The Mann-Kendall (MK) trend test (Mann, 1945; Kendall, 1975; Gilbert, 1987) is used to examine the trend significance, and the Theil-Sen trend estimate method (Sen, 1968) is used to estimate the slope of trend, which could also be considered as the rate of change, during the six-year period. Compared to the linear fitting analysis which require data to be independent and follow a Gaussian distribution, the non-parametric trend test methods only need the data be independent (Gocic and Trajkovic, 2013). To determine if the calculated rate of change is statistically significant, the confidence level of at least 95% is adopted in the MK trend test, with α value less than 0.05 being considered a statistically significant trend. The trend significance is examined by comparing the value of a standardized test statistic Z to that of a standard normal variate at a given significance level (Z_α, α=0.05). If $|Z| > Z_{1-\alpha/2}$, then the dataset is non-stationary, exhibiting either an increasing or a declining trend; If $|Z| \leq Z_{1-\alpha/2}$, then the dataset is stationary with no significant trend. Detailed calculation of Z can be referred to Xu et al. (2016).

3 Results and discussion

3.1 Regional transport characteristics at SSI

The observed O_3 concentrations at SSI were inevitably influenced by regional transport depending on the prevailing winds in various seasons. Figure 2 displays the monthly wind rose diagrams averaged over the period of 2012 to 2017 at DT. As mentioned in Sect. 2.2, the DT site is a rural site located quite close to SSI. The observed wind speeds and wind directions could then be applied to deduce the origins of the air mass arriving at SSI in adjacent region. Generally, observed prevailing winds exhibited distinct seasonal variabilities which were greatly affected by the East Asian monsoon. In warm seasons (May-August), the site was predominately influenced by easterly and southeasterly winds, accounting for 40–50% of the total winds. While in cold seasons (November-February), the northwesterly and northerly winds became the predominant flows that affected SSI, accounting for about 45% of total winds. During transitional months (e.g. March, April, September and October), the dominant winds presented more diversities, with wind directions dispersedly distributed in all the directions. The observed seasonal variations of prevailing winds are typical at coastal cities at mid-latitude region (Shan et al., 2016; Xu et al., 2019), suggesting that air masses arriving at SSI originated from various regions and could result in different impacts on the offshore atmospheric composition in different months.

Since CO has a relative long chemical lifetime of a few months, the observed CO concentrations at DT could be regarded as a consequence of regional transport from polluted regions (Tie et al., 2009). Figure 3 displays the observed monthly mean CO mixing ratios under wind directions of north (N), northeast (NE), east (E), southeast (SE), south (S), southwest (SW), west (W), and northwest (NW) at DT during the 2012–2017 period. Observed CO exhibited relative higher concentrations under SW and W winds in all months, with mean mixing ratios of 0.44 and 0.56 ppmv, respectively during 2012–2017

https://doi.org/10.5194/acp-2020-681
Preprint. Discussion started: 12 August 2020

(Table 1). The observed high CO mixing ratios suggested that the atmosphere constituents at SSI could be more affected by regional transport of air pollutants under SW and W wind conditions. As SSI is located to the northeast of the Shanghai city (Fig. 1), air masses carried by the SW and W flows usually contain more urban pollutants from upwind city areas, and those carried by E, SE, and NE flows mostly come from the ocean. The oceanic air masses are cleaner compared to those from the cities, leading to lower CO mixing ratio at SSI. For example, observed CO exhibited a mean concentration of 0.23 ppmv under SE wind conditions, which was about 50% lower than that influenced by W winds. To further examine the impacts of the SW and W winds on the atmosphere constituents at SSI, Table 2 lists the calculated monthly mean occurrence frequency of the SW and W winds in separate months during the studied period. The SW and S winds were most infrequent in September (6.1 %) and October (5.2 %), suggesting that the atmosphere at SSI during the two months could be less contaminated by pollutants transported from the city and might be more close to the baseline oceanic air conditions.

3.2 The diurnal pattern of ozone at SSI

Figure 4 displays the monthly mean diurnal variations of O_3 at SSI and XJH in different months during 2012–2017. The observed O_3 concentrations at the two sites exhibited similar seasonal distinctions, with monthly mean values highest (61.4 ppbv for SSI and 35.9 ppbv for XJH) in May and lowest (33.4 ppbv for SSI and 12.5 ppbv for XJH) in December. Since the O_3 formation in urban Shanghai is VOC-limited, observed O_3 could be significantly depressed by large NO_x emissions at downtown site (XJH) (Gu et al., 2020). In Fig. 4, observed O_3 levels at XJH were quite lower than those at SSI in all

https://doi.org/10.5194/acp-2020-681
Preprint. Discussion started: 12 August 2020

months, with mean concentrations of 27.8 and 50.1 ppbv, respectively at XJH and SSI during the observation period. The observed mean O_3 concentration at the rural site of DT (44.7 ppbv) was also lower than that at SSI, which suggested that the O_3 levels in marine air were higher than the continental O_3 at both urban and rural sites. The observed diurnal patterns of O_3 at SSI and XJH were similar to those reported for other sites in eastern China (Xu et al., 2008; Geng et al., 2015; Gao et al., 2017), exhibiting minimums in early morning (06:00–08:00 LST) and maximums in the afternoon (13:00–15:00 LST). However, compared to those at the urban site (XJH), observed amplitudes of O_3 diurnal variations were much smaller at SSI. The diurnal variations of surface O_3 can be mainly attributed to the O_3 production through photochemical reactions in the daytime and O_3 depression via NO titration at nighttime (Sillman, 2003). Due to few emissions of O_3 precursors (NO_x and VOCs), the O_3 production and depression could be weaker at remote site, resulting in flatter diurnal cycle of O_3 compared to that at polluted urban site.

Since the amplitudes of O_3 diurnal variations usually exhibited much smaller values in background areas compared to those in polluted urban regions, the ratio of daily maximum O_3 concentration ($O_{3\text{-max}}$) to minimum O_3 concentration ($O_{3\text{-min}}$) was regarded as an indicator to identify if the local O_3 pollution was significantly influenced by anthropogenic emissions (Cvitas and Klasinc 1993; Vingarzan, 2004). The $O_{3\text{-max}}/O_{3\text{-min}}$ ratio displayed larger values in polluted regions (Cvitas et al., 1995) and lower values in less contaminated rural regions. A ratio of about 1.4 suggested that the site could be regarded as a typical background site (Scheel et al., 1997). In Fig. 4, observed O_3 displayed different diurnal variabilities in different months, indicating different influence of regional transport on O_3 levels at SSI. Figure 5 displays the calculated monthly mean $O_{3\text{-max}}/O_{3\text{-min}}$ ratios at SSI and XJH, respectively during 2012–2017. Generally, the observed ratios of $O_{3\text{-max}}/O_{3\text{-min}}$ at SSI were much lower than those at XJH in all the months, suggesting less impact of anthropogenic emissions on O_3 levels. The calculated mean ratios were 3.03 and 5.20, respectively at SSI and XJH, and most of the calculated values were larger than 4.50 at the urban site. Besides, the ratios presented distinct seasonal differences at XJH and SSI sites. Higher values were observed in summer, indicating stronger photochemical production of daytime O_3 during June to August. At SSI, the $O_{3\text{-max}}/O_{3\text{-min}}$ ratio exhibited relatively low values in September and October, ranging from 1.61–2.35 during the studied period. Since the observed temperature and solar radiation still exhibited higher values during the two months in Shanghai (Gao et al., 2017), the observed low O_3 diurnal amplitudes should not be attributed to the weakened photochemical formation of O_3 as those in winter. Due to the persistent control of anticyclone, Shanghai and its neighboring areas are usually dominated by stable weather conditions in September and October, resulting in more gentle and diversified wind conditions. During the two months, the occurrences of more polluted SW and W winds were lowest (6.1% and 5.2%) throughout the year. The corresponding wind speed (2.49 and 2.50 m s^{-1}) also exhibited values 20% lower those in other months (Table 2). The transport conditions led to fewer pollutants transported to the SSI region, which could explain the observed weak diurnal variabilities of O_3 in September and October. The transport conditions together with O_3 response further confirmed that the transport of city pollutants had minimum impacts on the offshore O_3 levels in oceanic air at SSI in

https://doi.org/10.5194/acp-2020-681
Preprint. Discussion started: 12 August 2020

September and October.

3.3 Overall changes of ozone in oceanic air at SSI

Several studies have observed increasing trends of ground-level O_3 in metropolitan areas over eastern China since 2013, suggesting that the O_3 increases were mostly attributed to the NO_x emission reductions (Ma et al., 2016; Gao et al., 2017; Lu et al., 2018; Li et al., 2019b). However, the O_3 changes at remote sites were relatively not well elucidated during past years. Figure 6a presents the monthly variations of O_3 concentrations at SSI and XJH during the 2012–2017 period. The statistical results of the MK test and Theil–Sen trend estimate method indicated that observed monthly mean O_3 mixing ratios ($O_{3\text{-ave}}$) exhibited increasing changes at both urban (XJH) and remote sites (SSI) in Shanghai, with calculated increasing rate of 1.97 and 1.12 ppbv yr^{-1}, respectively in XJH and SSI. Though an overall upward trend of O_3 was detected at SSI, the changes were not as remarkable as those observed at XJH, which could not even pass the MK trend test at the 90% confidence level. The detected increasing trend of O_3 in oceanic air at SSI were also not as remarkable as those observed at remote continental sites (e.g. DT and Lin'an) over the Yangtze River Delta (YRD) region (Xu et al., 2008; Gao et al., 2017; Gu et al., 2020), suggesting few influence of anthropogenic emissions on the observed O_3 levels in oceanic air.

As discussed in Sect. 3.1, different prevailing winds led to different transport conditions at SSI in various months. Comparatively, the observed O_3 concentrations at SSI were least contaminated by the regional transport of air pollutants in September and October. To further examine the changes of nearly uncontaminated O_3, we present the

https://doi.org/10.5194/acp-2020-681
Preprint. Discussion started: 12 August 2020

variations of daily mean surface O_3 mixing ratios in September and October at SSI and XJH, respectively during the six-year period in Fig. 6b. The corresponding mean O_3 mixing ratios were 60.9 and 31.3 ppbv, respectively at SSI and XJH. Compared to the significant increasing changes of O_3 (0.59 ppbv yr^{-1}, $\alpha<0.05$) at urban site (XJH), observed O_3 at SSI in September and October exhibited insignificant decreasing changes during the studied period, with an average rate of -0.72 ppbv yr^{-1}. The changes were smaller and quite different from the overall changes at SSI as well as those detected at XJH, which further indicated that the observed O_3 levels at SSI in September and October should be seldom influenced by urban plumes, providing a good proxy to study the baseline O_3 and oxidation capacity of background atmosphere in eastern China.

To investigate possible drivers of the observed changes in the least contaminated O_3 concentrations in September and October at SSI, Table 3 displays the statistical results of the MK test and Theil-Sen trend estimate for NO_x, CO mixing ratios, temperature, and wind speed during the 2012–2017 period. Statistically significant upward trends were detected in NO_x concentrations and wind speed with estimated increasing rates of 0.48 ppbv yr^{-1} and 0.21 m s^{-1} yr^{-1}, respectively during the observation period ($\alpha<0.05$). The results suggested that increases in surface wind speed might be an important meteorological driver of the observed decreasing changes in O_3 levels at SSI from 2012 to 2017. Since both NO_x and CO levels exhibited different increases, it means more pollutants could be transported to the island and might resulted in elevated O_3 depressions during the period. Figure 6c presents corresponding variations of daytime and nighttime mean O_3 concentrations at SSI. Similarly, insignificant downward changes were detected in both daytime and nighttime O_3 levels, indicating that the diffusion and depression of O_3 might be enhanced at SSI due to elevated wind speeds and NO_x concentrations. Since observations of solar radiation were not available during the study period, the influence of radiation cannot be analyzed which might also play important role in determining the overall changes of the observed O_3 at SSI.

3.4 Impacts of urban plumes on ozone in oceanic air at SSI

Due to the relatively long residence lifetime (about one month), O_3 produced at urban regions could be transported several hundred kilometers away to downwind areas. Meanwhile, the urban plumes become more aged with continuous production/depletion of O_3 and its precursors, resulting in non-linear variations of O_3 in downwind areas (Geng et al., 2011; Tie et al., 2009, 2013). Several studies suggested that there tended to be considerable O_3 formations in aged urban plumes in the downwind region of Shanghai (Geng et al., 2011; Tie et al., 2013). To investigate the impacts of urban plumes on the O_3 levels in oceanic air at SSI, the relationships between observed O_3 and NO_x under different wind conditions at SSI and DT are investigated in this section.

Figure 7 presents the daytime and nighttime O_3/NO_x-wind relationships in MAM (March–May), JJA (June–August), SON (September–November), and DJF (December–February), respectively during 2012–2017. The SW and W winds were associated with higher NO_x concentrations in both daytime and nighttime. The result is consistent with the observed CO changes in Sect. 3.1. Since there is no local anthropogenic emission at SSI, the higher levels of NO_x and CO were mainly resulted from the transport of more polluted urban plumes by the SW and W winds. Generally, observed daytime O_3 and NO_x

concentrations presented opposite variations with the wind direction changes (Fig. 7a). In SON and DJF, the correlation coefficients (Rs) between daytime O_3 and NO_x were -0.72 and -0.75, respectively, indicating that the O_3 formation was inhibited by increased NO_x concentrations. The results are in accordance with Tie et al. (2013), who suggested that the VOC-limited regime of O_3 formation was not only confined in urban Shanghai, but also extended to a broader regional area surrounding Shanghai. However, in MAM and JJA, the daytime O_3-NO_x variations presented totally different patterns under SW and W wind conditions. As wind directions turned from E-SE to SW-W, observed mean NO_x concentrations increased from about 10 ppbv to 20 ppbv, while observed mean O_3 concentrations increased from 50–60 ppbv to 70–80 ppbv. The enhancements in daytime O_3 levels suggested that there should be persistent production of O_3 in the polluted air masses carried by the SW and W winds in MAM and JJA.

Based on observations and WRF-Chem simulations, Tie et al. (2013) suggested considerable O_3 production in aged city plumes in the downwind area of Shanghai. Since air masses affecting SSI site were directly originated from Shanghai under the SW and W wind conditions (Fig. 1), the observed O_3 enhancements should be mainly attributed to the O_3 production in the city plumes carried by SW and W winds. Studies during the MIRAGE-Shanghai campaign suggested several factors that contributed to the O_3 enhancements in aged city plumes downwind Shanghai. First, as there is a large area of forest located in the south of Shanghai, Geng et al. (2011) suggested that continuous oxidation of isoprene emitted by the biogenic sources could result in enhanced production of hydrogen radicals (HO_2) especially in warm seasons. Once the air massed were transported north and mixed with high NO_x emissions, O_3 would be quickly produced. However, the impacts of biogenic emissions on O_3 production were mainly limited in the south part of Shanghai, which can hardly influence the atmosphere in the SSI region. Then, Tie et al. (2013) further illustrated that the OH reactivity of alkane, alkene, aromatics, and oxygenated VOCs (OVOCs) contributed to the O_3 formation in city plumes. Among them, the influence of alkane, alkene and aromatics mostly occurred within or near the city, while the OVOCs could be produced or emitted during the transport of the city plumes, resulting in substantial O_3 enhancements in aged city plumes at 100–200 km downwind Shanghai.

The SSI is located approximately 100 km northeast from the downtown area of Shanghai. In MAM and JJA, the SW and W winds carried air masses with enhanced OVOCs oxidation and O_3 production, resulting in elevated daytime O_3 levels on the island. While in SON and DJF, the observed O_3 decreases at SSI during SW and W winds suggested lower efficiency of O_3 productivity in the city plumes. That might be because that fewer OVOCs were released or produced downwind the city due to the lower temperature and weaker solar radiation (Cai et al., 2009). In addition, in SON and DJF, the SW and W winds were usually related to low pressure system with large cloud cover and rich water vapor in Shanghai, which could also lead to depressed photochemical reactions and decreased O_3 levels. At night, observed O_3 and NO_x displayed totally opposite changes with wind directions (Fig. 7b), indicating O_3 depression by nighttime NO_x titration in all the seasons. High O_3 levels were observed under northeasterly, easterly and southeasterly oceanic wind conditions, ranging from 50–60, 30-55, 55–60, and 40–50 ppbv respectively at night in MAM, JJA, SON, and DJF. More detailed measurements are still needed to further understand the impacts of city plumes on the O_3 levels in oceanic air.

3.5 Impacts of offshore ozone on urban ozone air quality in Shanghai

As is presented in Sect. 3.2 and 3.3, observed O_3 concentrations at SSI were much higher than those at urban site (XJH), suggesting higher levels of O_3 in oceanic air than those on the continent. Therefore, sea breezes tend to bring more O_3 to the continent, aggravating O_3 pollution in coastal cities. Shanghai is one of the largest cities located on the east coast of China, experiencing severe O_3 pollution in recent years (Xu et al., 2019; Gu et al., 2020). The easterly winds from the ocean greatly affect the Shanghai region, accounting for 64–78 % of the total flows in non-winter months during the period 2012–2017. To understand the impacts of higher O_3 in oceanic air on the urban air quality, numerical experiments are conducted using the WRF-Chem model to examine the response of O_3 levels in Shanghai to various oceanic air inflow conditions in this section.

Simulations are performed during September 1–30 2014 when the prevailing winds were mostly northeasterly and easterly in the Shanghai region. The occurrence frequencies of the northeasterly and easterly winds were 23% and 27% respectively, during the simulation period, suggesting dominant influence of the oceanic air inflows on the city of Shanghai. Consistent with above analysis, observed air O_3 concentrations were much higher in oceanic regions than those in city areas, with monthly mean values of 30.9 and 57.7 ppbv, respectively at XJH and SSI in September 2014. The chemical boundary conditions (BCs) of the regional model can represent the inflows conditions to explore

https://doi.org/10.5194/acp-2020-681
Preprint. Discussion started: 12 August 2020

their impacts on surface concentrations of air pollutants over a certain continent region. Using this method, Pfiter et al. (2011) proposed that chemical inflows taken from different observational and model datasets could result in differences of ±15 ppbv in O_3 levels in the US west coast region. Therefore, three sets of numerical experiments are conducted as follows to access the impacts of oceanic O_3 air inflows on the urban O_3 air quality in Shanghai. All the simulations are driven by the same emissions, initial conditions, physical and chemical schemes.

(1) BC_40: O_3 concentrations at the eastern lateral boundary of the domain on the ocean are assigned to 40 ppbv, which is provided by the MOZART-4 model, closed to the observed urban O_3 levels (29.0–38.4 ppbv) in Shanghai in September. The chemical BCs are updated every 6 hours.

(2) BC_50: Same as BC_40, but with O_3 concentrations setting to 50 ppbv at the eastern lateral boundary of the domain.

(3) BC_60: Same as BC_40, but with O_3 concentrations at the eastern lateral boundary of the domain setting to 60 ppbv according to the observed O_3 levels at SSI (50.9–71.0 ppbv) in September.

Figure 8 displays the simulated monthly mean distributions of surface O_3 concentrations in BC_40, BC_50 and BC_60 scenarios, respectively. The calculated distributions of O_3 agree with observations, which exhibit lower values in urban regions compared to those in rural and ocean areas, indicating strong O_3 depressions in the city of Shanghai due to the VOC-limited O_3 formation regime. The R values between the simulated and observed O_3 concentrations are all larger than 0.50 at XJH, suggesting

https://doi.org/10.5194/acp-2020-681
Preprint. Discussion started: 12 August 2020

good prediction of O_3 variations by the model. Table 4 displays the statistical results of the comparisons between the simulated and observed surface O_3 concentrations at SSI and XJH, respectively. Generally, the WRF-Chem model underestimates O_3 concentrations at both XJH and SSI site. Taken the BC_40 scenario for example, the O_3 concentrations are underestimated by 27% and 36% respectively at XJH and SSI, suggesting larger underestimation of O_3 concentrations in ocean regions. Model results suggest that increases in the eastern boundary O_3 lead to increases in O_3 concentrations at both urban and remote sites when the prevailing winds are mostly easterly in Shanghai. With O_3 concentrations increasing from 40 to 60 ppbv in the easterly inflows, the simulated monthly mean O_3 concentrations increase by 7.0 and 10.4 ppbv, respectively at XJH and SSI. The underestimation of O_3 levels by the model is also significantly improved in the BC_60 scenario, with the chemical BCs of O_3 more close to the observed chemical inflow conditions. Compared to those in the BC_40 scenario, the normalized mean bias (NMBs) of the predicted O_3 concentrations reduced from -36.1 % to -18.1 % at SSI and -27.6% to -4.6% at XJH in the BC_60 scenario, suggesting a crucial role of the eastern oceanic air inflows in influencing O_3 air quality in Shanghai.

The calculated monthly mean differences in surface O_3 concentrations between simulations in different scenarios are further presented in Fig. 9. Since the dominant winds are easterly during the simulation period, distinct changes in surface O_3 concentrations throughout Shanghai are generated, exhibiting generally gradient increases from the ocean to the continent as O_3 increases in the oceanic air inflows. With every 10 ppbv increases in O_3 levels in oceanic air, the simulated surface mean O_3 concentrations

https://doi.org/10.5194/acp-2020-681
Preprint. Discussion started: 12 August 2020

increase by 3–6 ppbv in the land area and 4–7 ppbv in the offshore region. Due to the strong O_3 depressions associated with high anthropogenic emissions, the simulated O_3 enhancements are relatively lower in the central urban region compared to those in surrounding areas. Even so, simulated mean O_3 concentrations still exhibit 6–8 ppbv increases in the BC_60 scenario, accounting for approximately 30% of the simulated O_3 concentrations in the BC_40 case. During the period 2012–2017, most of the measured O_3 concentrations ranged between 50—60 ppbv at SSI in non-winter seasons. Carried by the easterly inflows, these oceanic air masses with higher O_3 levels (50—60 ppbv) could be transported to the coastal regions, resulting in approximately 20—30% increases in urban O_3 concentrations in Shanghai according to the sensitivity results.

4 Conclusions

In this paper, we present the first relatively long and continuous measurements of oceanic air O_3 conducted at an offshore monitoring station on the Sheshan Island during January 1 2012 to September 15 2017.The southwesterly and westerly winds are proved to carry more pollutants to the SSI site, exerting greater influence of human activities on the oceanic atmosphere over the offshore region of the East China Sea. Since the two kinds of winds exhibited minimum occurrence frequencies and wind speeds in September and October, atmosphere at SSI during the two months are considered to be less affected by the transport of regional pollution.

Compared to those in urban (XJH) and rural (DT) sites, the observed O_3 levels were higher at SSI, with mean concentrations of 50.1 ppbv during the observation period. Similar seasonal and diurnal patterns of O_3 were observed at SSI and XJH; however, the amplitudes of O_3 variations were much smaller at the offshore site (SSI). Since O_3 formation in Shanghai and its surrounding regions were VOC-limited, the observational results suggested that the production and depression of O_3 could be weaker in the ocean regions due to weak influence of the anthropogenic emissions. Observed mean $O_{3\text{-max}}/O_{3\text{-min}}$ ratios also exhibited lower values at SSI (3.03) than those at XJH (5.20), with minimum values ranging from 1.61–2.35 in September and October. The result further illustrated that SSI was seldom affected by the anthropogenic emissions, especially in September and October.

The multi-year changes of the oceanic O_3 at SSI are investigated using the Mann-Kendall trend test and the Theil-Sen trend estimate method during 2012–2017. Different from the significant O_3 increases detected at XJH and other rural sites reported in previous studies, the observed mean O_3 concentrations at SSI exhibited statistically insignificant increasing changes (1.12 ppbv yr^{-1}, $\alpha>0.10$) during the observation period and insignificant decreasing changes (-0.72 ppbv yr^{-1}, $\alpha>0.10$) in September and October when the transport of city pollutants had minimum impacts on the island. Due to fewer impacts of anthropogenic emissions, most of the observed changes in O_3 at SSI could be attributed to the changes of meteorological parameters. Observed wind speed exhibited significant increases (0.21 m s^{-1}, $\alpha>0.10$) in September and October during the observation period, suggesting that enhanced diffusion conditions could be an important meteorological factor in determining the decreases in O_3 concentrations during the observation period.

The impacts of urban plumes on O_3 levels in oceanic air at SSI are evaluated by studying the relationships between observed O_3 and NO_x under different wind conditions. The SW and W winds usually carried air masses with higher NO_x concentrations in both daytime and nighttime to the island. Generally, observed daytime and nighttime O_3 concentration decreased as NO_x concentration increases in SW and W winds, exhibiting typical VOC-limited characteristics of O_3 formation. The pattern was more typical in SON and DJF, with R values of -0.72 and -0.75, respectively between O_3 and NO_x concentrations. In MAM and JJA, the daytime O_3-NO_x variations presented kind of positive relationships under SW and W wind conditions, suggesting continuous O_3 production in aged city plumes from Shanghai. As reported in previous studies during the MIRAGE-Shanghai campaign, enhanced OVOCs oxidation should be the most important driver of the observed O_3 enhancements in the city plumes transported by the SW and W winds.

The influence of the oceanic O_3 air inflows on urban O_3 air quality in Shanghai are quantified during an easterly wind dominant episode (September 1–30, 2014). Numerical experiments are conducted with chemical BCs of O_3 assigned according to different inflow conditions using the WRF-Chem model. Model results suggest that increases of O_3 in the easterly oceanic air inflows will lead to gradient increases from the ocean to the continent. With every 10 ppbv O_3 increases, the calculated surface mean O_3 concentrations can increase by 3–6 ppbv in the land and 4–7 ppbv in the offshore region. Compared to those in surrounding regions, O_3 in central city of Shanghai exhibited lower enhancements in response to the O_3 increases in oceanic air inflows due to strong O_3 depression processes. Even so, the impacts of the oceanic air inflows can still lead to 20—30% increases in urban O_3 concentrations which should be crucially considered in dealing with O_3 pollution in large coastal cities like Shanghai.

Data availability. The data used in this paper can be provided upon request from Dr. Jianming Xu (metxujm@163.com).

Author contribution. YG and JX came up with the original idea, designed the analysis methods, developed the model code, and performed the simulations. WG provided the observational data. YG and YQ conducted the analysis of the observations and model results. YG prepared the manuscript with contributions from all co-authors.

Competing interest. The authors declare that they have no conflict of interest.

Acknowledgements. This work was supported by Shanghai Sailing program (18YF1421200) and Science and Technology Commission of Shanghai Municipality (Grand No. 19DZ1205003).

Reference

Cai, C., Geng, F., Tie, X. X., Yu, Q., and An, J.: Characteristics and source apportionment of VOCs measured in Shanghai, China, Atmos. Environ., 44, 5005–5014, 2010.

Chen, F. and Dudhia, J.: Coupling an advanced land surface hydrology model with the Penn State-NCAR MM5 modeling system, Part I: Model implementation and sensitivity, Mon.Weather Rev., 129, 569–585, 2001.

Cvitas, T., and Klasinc, L.: Measurement of tropospheric ozone in the Eastern Mediterranean, Boll. Geofisico, 16, 521–527, 1993.

Cvitas, T., Kezele, N., Klasinc, L., and Lisac, J.: Tropospheric ozone measurements in Croatia, Pure Appl. Chem., 67, 1450–1453,1995.

Dudhia, J.: Numerical study of convection observed during the winter monsoon experiment using a mesoscale two-dimensional model, J. Atmos. Sci., 46, 3077–3107, 1989.

Emmons, L. K., Walters, S., Hess, P. G., Lamarque, J.-F., Pfister, G. G., Fillmore, D., Granier, C., Guenther, A., Kinnison, D., Laepple, T., Orlando, J., Tie, X., Tyndall, G., Wiedinmyer, C., Baughcum, S. L., and Kloster, S.: Description and evaluation of the Model for Ozone and Related chemical Tracers, version 4 (MOZART-4), Geosci. Model Dev., 3, 43–67, https://doi.org/10.5194/gmd-3-43-2010, 2010.

Fountoukis, C., and Nenes, A.: ISORROPIA II: a computationally efficient aerosol thermodynamic equilibrium model for K^+, Ca^{2+}, Mg^{2+}, NH_4^+, Na^+, SO_4^{2-}, NO_3^- , Cl^-,H_2O aerosols. Atmos. Chem. Phys. 7, 4639–4659, 2007.

Gao, W., Tie, X., Xu, J., Huang, R., Mao, X., Zhou, G., and Chang, L.: Long-term trend of O_3, in a mega city (Shanghai), China: characteristics, causes, and interactions with precursors, Sci. Total Environ., 603–604, 425–433, 2017.

Geng, F., Mao, X., Zhou, M., Zhong, S., and Lenschow, D.: Multi-year ozone concentration and its spectra in Shanghai, China, Sci. Total Environ., 521–522, 135–143, 2015.

Geng, F., Tie, X., Guenther, A., Li, G., Cao, J., and Harley, P.: Effect of isoprene emissions from major forests on ozone formation in the city of Shanghai, China, Atmos. Chem. Phys., 11, 10449–10459, 2011.

Gilbert, R.O.: Statistical Methods for Environmental Pollution Monitoring. John Wiley & Sons, New York, USA, 1987.

Goodman, J. E., Prueitt, R. L., Sax, S. N., Pizzurro, D. M., Lynch, H. N., Zu, K., and Venditti, F. J.: Ozone exposure and systemic biomarkers: evaluation of evidence for adverse cardiovascular health impacts, Crit. Rev. Toxicol., 45, 412–452, 2015.

Grell, G. A., Peckham, S. E., Schmitz, R., McKeen, S. A., Frost, G., Skamarock, W. C., and Eder, B.: Fully coupled “online” chemistry within the WRF model, Atmos. Environ., 39, 6957–6975, 2005.

Gocic, M., Trajkovic, S.: Analysis of changes in meteorological variables using Mann-Kendall and Sen’s slope estimator statistical tests in Serbia, Global Planet. Change, 100, 172–182, 2013.

Gu, Y., Li, K., Xu, J., Liao, H., Zhou, G.: Observed dependence of surface ozone on increasing temperature in Shanghai, China. Atmos. Environ., 221, 117108, 2020.

Guenther, A., Karl, T., Harley, P., Wiedinmyer, C., Palmer, P. I.,, and Geron, C.: Estimates of global terrestrial isoprene emissions using MEGAN (model of emissions of gases and aerosols from nature), Atmos. Chem. Phys., 6, 3181–3210, 2006.

Hong, S. Y. and Lim, J. O. J.: The WRF Single-Moment 6-Class Microphysics Scheme (WSM6), J. Korean Meteor. Soc., 42, 129–151, 2006.

IPCC: Climate Change 2013: The Physical Science Basis. Contribution of Working Group I to the Fifth Assessment Report of the Intergovernmental Panel on Climate Change, edited by Stocker, T. F., Qin, D., Plattner, G. K., Tignor, M., Allen, S. K., Boschung, J., Nauels, A., Xia, Y., Bex, V. and Midgley, P. M.,, Cambridge University Press, United Kingdom and New York, USA, 2013.

Kendall, M.G.: Rank Correlation Methods, fourth ed., Charles Griffin, London, 1975.

Li, K., Jacob, D.J., Liao, H., Zhu, J., Shah, V., Shen, L., Bates, K.H., Zhang, Q., and Zhai, S.: A two-pollutant strategy for improving ozone and particulate air quality in China. Nat. Geosci. https://doi.org/10.1038/s41561-019-0464-x, 2019a.

Li, K., Jacob, D. J., Liao, H., Shen, L., Zhang, Q., and Bates, K.H.: Anthropogenic drivers of 2013–2017 trends in summer surface ozone in China, P. Natl. A. Sci. USA 116 (2), 422–427, 2019b.

Li, M., Zhang, Q., Streets, D., He, K. B., Cheng, Y. F., Emmons, L. K., Huo, H., Kang, S. C., Lu, Z., Shao, M., Su, H., Yu, X., and Zhang, Y.:. Mapping Asian anthropogenic emissions of non-methane volatile organic compounds to multiple chemical mechanisms. Atmos. Chem. Phys. 14, 5617–5638, 2014.

Lin, M., Horowitz, L. W., Cooper, O. R., Tarasick, D., Conley, S., Iraci, L. T., Johnson, B., Leblanc, T., Petropavlovskikh, I., and Yates, E. L: Revisiting the evidence of increasing springtime ozone mixing ratios in the free troposphere over western North America, Geophys. Res. Lett., 42, 8719–8728, https://doi.org/10.1002/2015GL065311, 2015.

Lin, Y. L., Farley, R. D., and Orville, H. D.: Bulk parameterization of the snowfield in a cloud model, J. Clim. Appl. Meteorol., 22, 1065–1092, 1983.

Lin, W., Xu, X., Zhang, X., Tang, J.:. Contributions of pollutants from North China Plain to surface ozone at the Shangdianzi GAW Station, Atmos. Chem. Phys., 8,5889–5898, 2008.

Lu, X., Hong, J., Zhang, L., Cooper, O.R., Schults, M. G., Xu, X., Wang, T., Gao, M., Zhao, Y., and Zhang, Y.: Severe surface ozone pollution in China: a global perspective, Environ. Sci. Technol. Lett.,5(8), 487, 194, 2018.

Ma, Z., Xu, J., Quan, W., Zhang, Z., Lin, W., and Xu, X.: Significant increase of surface ozone at a rural site, north of eastern China, Atmos. Chem. Phys. ,16, 3969–3977, 2016.

Madronich, S., and Flocke, S.: The role of solar radiation in atmospheric chemistry, in: Handbook of Environmental Chemistry, edited by Boule, P.. Springer, Heidelberg, 1–26, https://doi.org/10.1007/978-3-540-69044-3_1, 1999.

Mann, H.B.: Non-parametric tests against trend, Econometrica 13, 163–171, 1945.

Meng, Z. Y., Xu, X. B., Yan, P., Ding, G. A., Tang, J., Lin, W. L., Xu, X. D., and Wang, S. F.: Characteristics of trace gaseous pollutants at a regional background station in Northern China, Atmos. Chem. Phys., 9, 927–936, https://doi.org/10.5194/acp-9-927-2009, 2009.

Monks, P. S., Archibald, A. T., Colette, A., Cooper, O., Coyle, M., Derwent, R., Fowler, D., Granier, C., Law, K.S., Mills, G.E., Stevenson, D.S., Tarasova, O., Thouret, V., von Schneidemesser, E., Sommariva, R., Wild, O., and Williams, M.L.: Tropospheric ozone and its precursors from the urban to the global scale from air quality to short-lived climate forcer, Atmos. Chem. Phys., 15, 8889-8973, 2015.

Pfister, G. G., Parrish, D. D., Worden, H., Emmons, L. K., Edwards, D. P., Wiedinmyer, C., Diskin, G. S., Huey, G., Oltmans, S. J., Thouret, V., Weinheimer, A., and Wisthaler, A.: Characterizing summertime chemical boundary conditions for airmasses entering the US West Coast, Atmos. Chem. Phys., 11, 1769–1790, 2011.

Scheel, H. E., Aresbough, H., Geiss, H., Gormiscek, B., Granby, K., Haszpra, L., Klasinc, L., Kley, D., Laurila, T., Lindskog, A., Roemer, M., Schmitt, R., Simmond, P., Solberg, S., and Toupande, G.: On the spatial distribution and seasonal variation of lower tropospheric ozone over Europe, J. Atmos. Chem., 28, 11–28,1997.

Schell, B., Ackermann, I., Hass, H., Binkowski, F. S., and Ebel, A.: Modeling the formation of secondary organic aerosol within a comprehensive air quality model system, J. Geophys. Res., 106, 28275–28293, https://doi.org/10.1029/2001JD000384, 2001.

Sen, P. K.: Estimates of the regression coefficient based on Kendall's tau, J. Am. Stat. Assoc., 63, 1379–1389, 1968.

Shan, W., Yang, P., Lu, H., Ma, K., and Huang, Z.: Influence of Coastal Wind on Surface Ozone and Nitrogen Oxides in Suburban Shanghai, Asia-Pac. J. Atmos. Sci., 52(5), 451–458, 2016.

Sillman, S.: Photochemical Smog: Ozone and its Precursors, in: Handbook of Weather, Climate, and Water, edited by Potter, T. and Bradley, R. R., John Wiley & Sons, New York, USA, 227–242, 2003.

Stockwell, W. R., Middleton, P., Chang, J. S., and Tang, X.: The second generation regional acid deposition model chemical mechanism for regional air quality modeling, J. Geophys. Res.-Atmos., 95, 16343–16367, 1990.

Tie, X., Brasseur, G., Emmons, L., Horowitz, I., and Kinnison, D.: Effects of aerosols on tropospheric oxidants: a global model study, J. Geophys. Res.-Atmos., 106, 22931–22964, 2001.

Tie, X., Geng, F., Guenther, A., Cao, J., Greenberg, J., Zhang, R., Apel, E., Li, G., Weinheimer, A., Chen, J., and Cai, C.: Megacity impacts on regional ozone formation: observations and WRF-Chem modeling for the MIRAGE-Shanghai field campaign, Atmos. Chem. Phys., 13, 5655–5669, 2013.

Tie, X., Geng, F., Peng, L., Gao, W., and Zhao, C.: Measurement and modeling of O_3 variability in Shanghai, China: Application of the WRF-Chem model, Atmos. Environ., 43, 4289–4302, 2009.

Tie, X., Madronich, S., Li, G. H., Ying, Z.M., Weinheimer, A., Apel, E., and Campos, T.: Simulation of Mexico City plumes during the MIRAGE-Mex field campaign using the WRF-Chem model, Atmos. Chem. Phys. 9, 4621–4638, 2009.

Tie, X., Madronich, S., Walters, S., Rasch, P., and Collins, W.: Effect of clouds on photolysis and oxidants in the troposphere, J. Geophys. Res., 108, 4642, 2003.

Vingarzan, R.: A review of surface ozone background levels and trends, Atmos. Environ., 38, 3431–3442, 2004.

Wang, T., Wei, X. L., Ding, A. J., Poon, C. N., Lam, Y. S., Li, Y. S., Chan, L. Y., and Anson, M.: Increasing surface ozone concentrations in the background atmosphere of Southern China, 1994–2007, Atmos. Chem. Phys., 9, 6217–6227, 2009.

Wang, T., Xue, L., Brimblecombe, P., Lam, Y.-F., Li, L., and Zhang, L.: Ozone pollution in China: A review of concentrations, meteorological influences, chemical precursors, and effects, Sci. Total Environ., 575, 1582–1596, 2017.

Wesely, M. L.: Parameterization of surface resistances to gaseous dry deposition in regional-scale numerical models, Atmos. Environ., 23, 1293–1304, 1989.

Xu, J., Tie, X., Gao, W., Lin, Y., and Fu, Q.: Measurement and model analyses of the ozone variation during 2006 to 2015 and its response to emission change in megacity Shanghai, China, Atmos. Chem. Phys., 19, 9017–9035, 2019.

Xu, X., Lin, W., Wang, T., Yan, P., Tang, J., Meng, Z., and Wang, Y.: Long-term trend of surface ozone at a regional background station in eastern China 1991–2006: enhanced variability, Atmos. Chem. Phys., 8, 2595–2607, 2008.

Xu, W., Lin, W., Xu, X., Tang, J., Huang, J., Wu, H., and Zhang, X.: Long-term trends of surface ozone and its influencing factors at the Mt Waliguan GAW station, China – part 1: overall trends and characteristics, Atmos. Chem. Phys., 16, 6191–6205, https://doi.org/10.5194/acp-16-6191-2016, 2016.

Yue, X. and Unger, N.: Ozone vegetation damage effects on gross primary productivity in the United States, Atmos. Chem. Phys., 14, 9137–9153, 2014.

Table 1 Mean CO mixing ratios (ppmv) under north (N), northeast (NE), east (E), southeast (SE), south (S), southwest (SW), west (W), northwest (NW) and calm (C) wind conditions at Dongtan (DT) site, a remote rural site near the Sheshan Island (SSI) during 2012 to 2017.

	N	NE	E	SE	S	SW	W	NW	C
CO	0.31	0.27	0.25	0.23	0.27	**0.44**	**0.56**	0.38	0.34

Table 2 Monthly mean wind speeds (m s^{-1}) and occurrence frequencies (%) of the southwest (SW) and west (W) winds at Dongtan (DT) site, a remote rural site near the Sheshan Island (SSI) during 2012 to 2017.

	Jan.	Feb.	Mar.	Apr.	May	Jun.	Jul.	Aug.	Sep.	Oct.	Nov.	Dec.
SW+W	11.5	9.2	11.9	13.2	12.7	9.8	17.7	10.8	**6.1**	**5.2**	11.9	15.1
Wind speed	2.70	2.93	2.98	3.04	2.86	2.51	2.65	2.77	**2.49**	**2.50**	2.55	2.54

Table 3 Statistical results of the Mann-Kendall test and Theil-Sen trend estimate for daily mean values of NO_x, CO mixing ratios, temperature (T), and wind speed (WS) in September and October at Dongtan (DT) site, a remote rural site near Sheshan Island (SSI) site during the 2012–2017 period. The units of the calculated slopes are ppbv yr^{-1} for NO_x and CO, ˚C yr^{-1} for T, and m s^{-1} yr^{-1} for WS.

	NO_x	CO	T	WS
Slope Estimate	0.48*	2.67^{Δ}	0.15^{Δ}	0.21*

[*] The result is significant at the 95% confidence level.

[Δ] The result cannot pass the Mann-Kendall trend test at the 90% confidence level.

Table 4 Statistical results of the comparisons between the simulated and observed surface O_3 concentrations at Xujiahua (XJH) and Sheshan Island (SSI) sites during September 2014. The calculated O_3 levels are obtained from BC_40, BC_50 and BC_60 simulations, respectively. Values of the average surface O_3 concentrations (Mean) and normalized mean bias (NMB) are displayed. The NMB is defined as NMB=$\frac{\sum_{i=1}^{n}(P_i-O_i)}{\sum_{i=1}^{n}O_i}$, where P_i and O_i are predicted and observed ozone mixing ratios for sample i, n is the number of total samples (numbers in parentheses).

	Cases	XJH (641)	SSI (720)
Mean (ppbv)	Observation	30.4	57.7
	BC_40	22.0	36.9
	BC_50	25.1	41.8
	BC_60	29.0	47.3
NMB (%)	BC_40	-27.6	-36.1
	BC_50	-17.5	-27.5
	BC_60	-4.6	-18.1

https://doi.org/10.5194/acp-2020-681
Preprint. Discussion started: 12 August 2020

Figure Captions

Figure 1 Land cover of Shanghai and corresponding locations and landscapes of Xujiahui (XJH, urban), Dongtan (DT, rural) and Sheshan Island (SSI, remote and oceanic) stations.

Figure 2 Monthly wind rose diagrams averaged over the period of 2012 to 2017 at Dongtan (DT) site, a remote rural site near the Sheshan Island (SSI).

Figure 3 Monthly mean CO mixing ratios under north (N), northeast (NE), east (E), southeast (SE), south (S), southwest (SW), west (W), northwest (NW) and calm (C) wind conditions at Dongtan (DT) site, a remote rural site near the Sheshan Island (SSI) during 2012 to 2017.

Figure 4 Monthly and year-round mean diurnal variations of O_3 (ppbv) at Sheshan Island (SSI, remote and oceanic) and Xujiahui (XJH, urban) sites during 2012 to 2017.

Figure 5 Calculated monthly mean ratios of daily maximum O_3 concentrations ($O_{3\text{-max}}$) to minimum O_3 concentrations ($O_{3\text{-min}}$) at Sheshan Island (SSI, remote and oceanic) and Xujiahui (XJH, urban) sites, respectively during 2012 to 2017.

Figure 6 Variations of (a) monthly mean O_3 concentrations at Sheshan Island (SSI, remote and oceanic) and Xujiahui (XJH, urban) sites during the period 2012–2017, (c) corresponding variations of daily mean O_3 concentrations at SSI and XJH in September and October, and (c) variations of mean O_3 concentrations during daytime (10:00-16:00 LST) and nighttime (23:00-04:00 LST) at SSI.

Figure 7 Daytime and nighttime mean O_3 mixing ratios (ppbv) at Sheshan Island (SSI) and NO_x mixing ratios (ppbv) at Dongtan (DT) site, a remote rural site near SSI under north (N), northeast (NE), east (E), southeast (SE), south (S), southwest (SW), west (W), and northwest (NW) wind conditions in MAM (March–May), JJA (June–August), SON (September–November), and DJF (December–February), respectively during 2012 to 2017.

Figure 8 Calculated distributions of monthly mean O_3 concentrations (shades, ppbv) from BC_40, BC_50 and BC_60 simulations, respectively in September 2014. Model results are compared with observed mean O_3 concentrations (circles, ppbv) obtained from Xujiahui (XJH, urban) and Sheshan Island (SSI, remote and oceanic) sites. Also shown is the calculated wind field (m s^{-1}) averaged over the same period.

Figure 9 Mean differences in surface O_3 concentrations (ppbv) simulated with different chemical boundaries: (a) BC_50 minus BC_40, (b) BC_60 minus BC_40, and (c) BC_60 minus BC_50 in September 2014. Also shown is the calculated wind field (m s^{-1}) averaged over the simulation period.

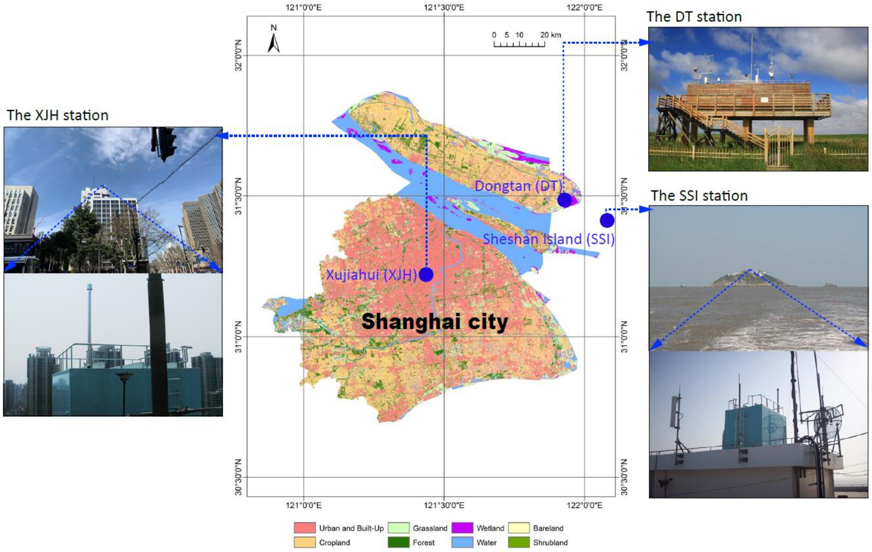

Figure 1 Land cover of Shanghai and corresponding locations and landscapes of Xujiahui (XJH, urban), Dongtan (DT, rural) and Sheshan Island (SSI, remote and oceanic) stations.

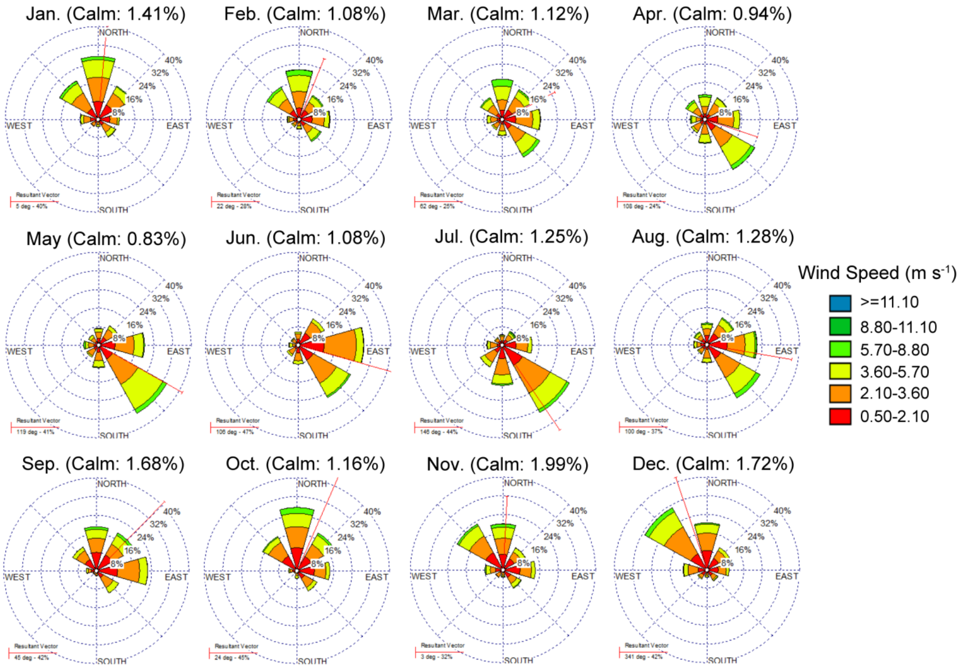

Jan. (Calm: 1.41%) Feb. (Calm: 1.08%) Mar. (Calm: 1.12%) Apr. (Calm: 0.94%)

May (Calm: 0.83%) Jun. (Calm: 1.08%) Jul. (Calm: 1.25%) Aug. (Calm: 1.28%)

Sep. (Calm: 1.68%) Oct. (Calm: 1.16%) Nov. (Calm: 1.99%) Dec. (Calm: 1.72%)

Figure 2 Monthly wind rose diagrams averaged over the period of 2012 to 2017 at Dongtan (DT) site, a remote rural site near the Sheshan Island (SSI).

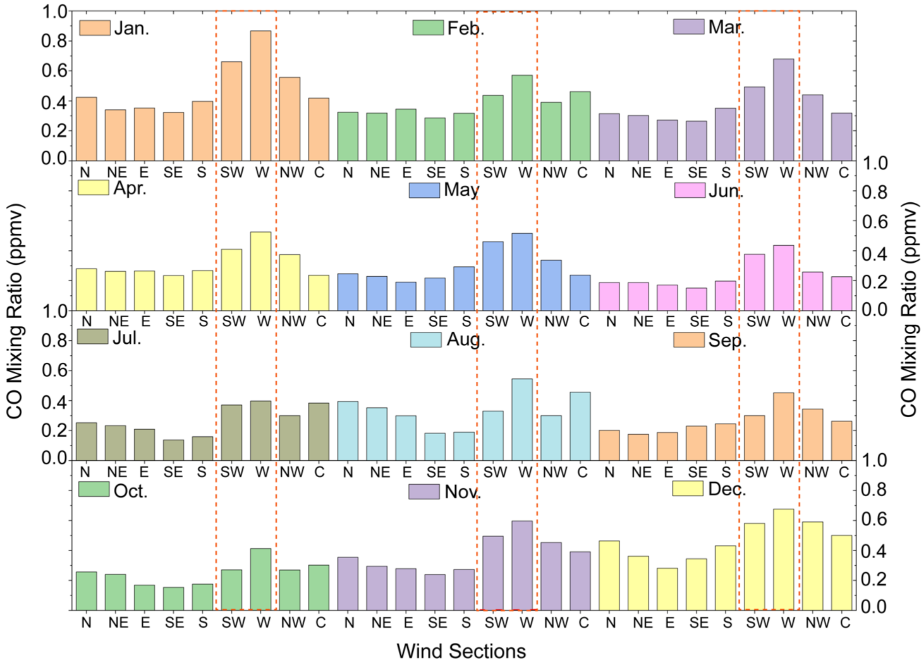

Figure 3 Monthly mean CO mixing ratios under north (N), northeast (NE), east (E), southeast (SE), south (S), southwest (SW), west (W), northwest (NW) and calm (C) wind conditions at Dongtan (DT) site, a remote rural site near the Sheshan Island (SSI) during 2012 to 2017.

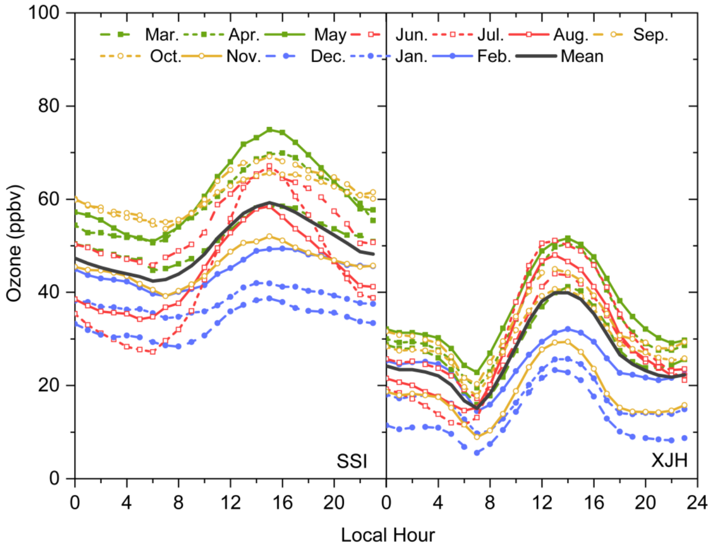

Figure 4 Monthly and year-round mean diurnal variations of O_3 (ppbv) at Sheshan Island (SSI, remote and oceanic) and Xujiahui (XJH, urban) sites during 2012 to 2017.

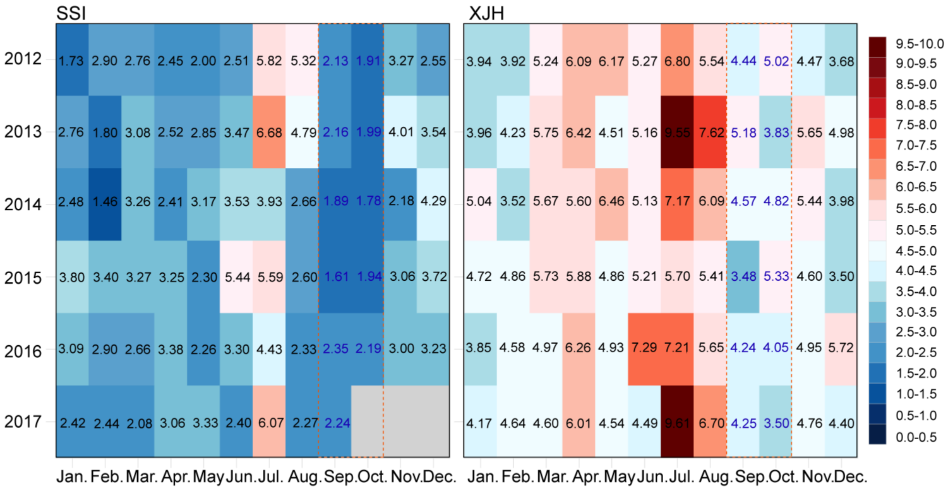

SSI

	Jan.	Feb.	Mar.	Apr.	May	Jun.	Jul.	Aug.	Sep.	Oct.	Nov.	Dec.
2012	1.73	2.90	2.76	2.45	2.00	2.51	5.82	5.32	2.13	1.91	3.27	2.55
2013	2.76	1.80	3.08	2.52	2.85	3.47	6.68	4.79	2.16	1.99	4.01	3.54
2014	2.48	1.46	3.26	2.41	3.17	3.53	3.93	2.66	1.89	1.78	2.18	4.29
2015	3.80	3.40	3.27	3.25	2.30	5.44	5.59	2.60	1.61	1.94	3.06	3.72
2016	3.09	2.90	2.66	3.38	2.26	3.30	4.43	2.33	2.35	2.19	3.00	3.23
2017	2.42	2.44	2.08	3.06	3.33	2.40	6.07	2.27	2.24			

XJH

	Jan.	Feb.	Mar.	Apr.	May	Jun.	Jul.	Aug.	Sep.	Oct.	Nov.	Dec.
2012	3.94	3.92	5.24	6.09	6.17	5.27	6.80	5.54	4.44	5.02	4.47	3.68
2013	3.96	4.23	5.75	6.42	4.51	5.16	9.55	7.62	5.18	3.83	5.65	4.98
2014	5.04	3.52	5.67	5.60	6.46	5.13	7.17	6.09	4.57	4.82	5.44	3.98
2015	4.72	4.86	5.73	5.88	4.86	5.21	5.70	5.41	3.48	5.33	4.60	3.50
2016	3.85	4.58	4.97	6.26	4.93	7.29	7.21	5.65	4.24	4.05	4.95	5.72
2017	4.17	4.64	4.60	6.01	4.54	4.49	9.61	6.70	4.25	3.50	4.76	4.40

Figure 5 Calculated monthly mean ratios of daily maximum O_3 concentrations ($O_{3\text{-max}}$) to minimum O_3 concentrations ($O_{3\text{-min}}$) at Sheshan Island (SSI, remote and oceanic) and Xujiahui (XJH, urban) sites, respectively during 2012 to 2017.

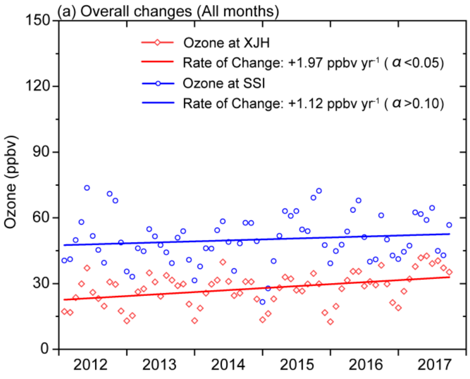
(a) Overall changes (All months)

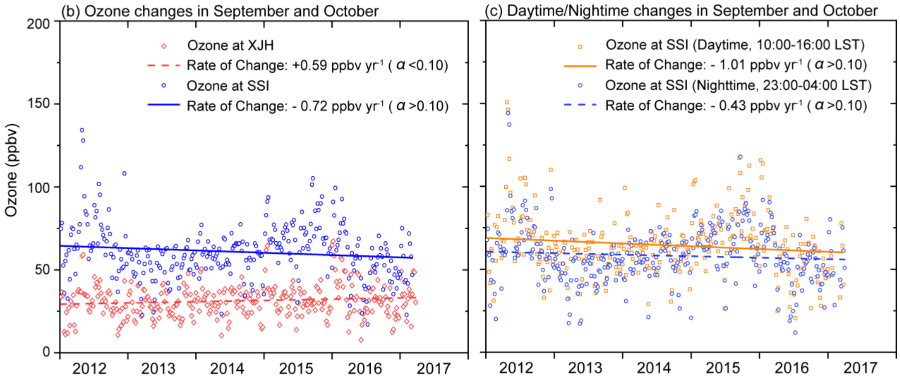
(b) Ozone changes in September and October

(c) Daytime/Nightime changes in September and October

Figure 6 Variations of (a) monthly mean O_3 concentrations at Sheshan Island (SSI, remote and oceanic) and Xujiahui (XJH, urban) sites during the period 2012–2017, (b) corresponding variations of daily mean O_3 concentrations at SSI and XJH in September and October, and (c) variations of mean O_3 concentrations during daytime (10:00-16:00 LST) and nighttime (23:00-04:00 LST) at SSI.

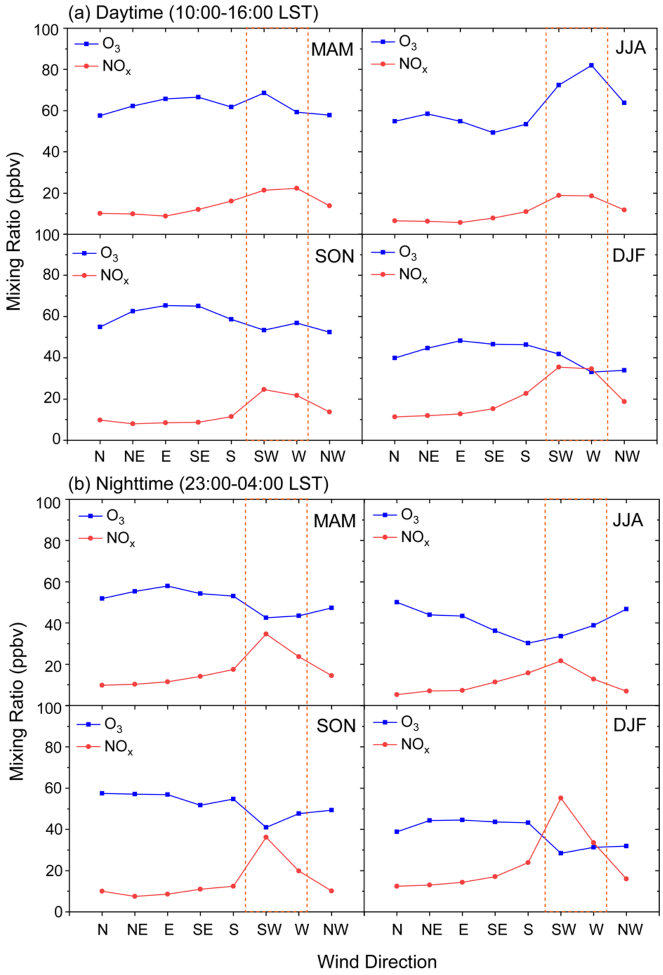

Figure 7 Daytime and nighttime mean O_3 mixing ratios (ppbv) at Sheshan Island (SSI) and NO_x mixing ratios (ppbv) at Dongtan (DT) site, a remote rural site near SSI under north (N), northeast (NE), east (E), southeast (SE), south (S), southwest (SW), west (W), and northwest (NW) wind conditions in MAM (March–May), JJA (June–August), SON (September–November), and DJF (December–February), respectively during 2012 to 2017.

https://doi.org/10.5194/acp-2020-681
Preprint. Discussion started: 12 August 2020

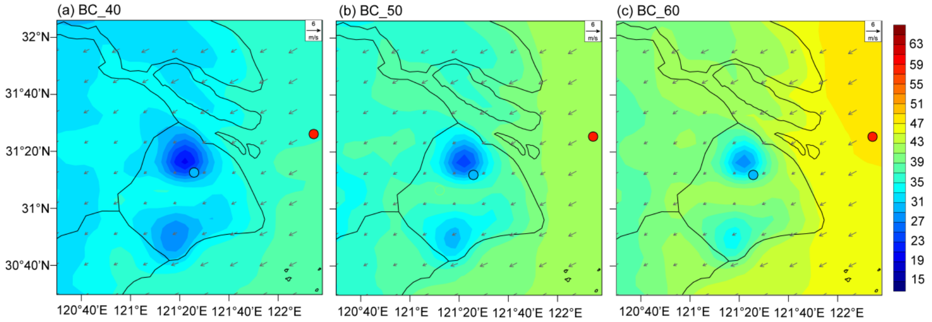

Figure 8 Calculated distributions of monthly mean O_3 concentrations (shades, ppbv) from BC_40, BC_50 and BC_60 simulations, respectively in September 2014. Model results are compared with observed mean O_3 concentrations (circles, ppbv) obtained from Xujiahui (XJH, urban) and Sheshan Island (SSI, remote and oceanic) sites. Also shown is the calculated wind field (m s^{-1}) averaged over the same period.

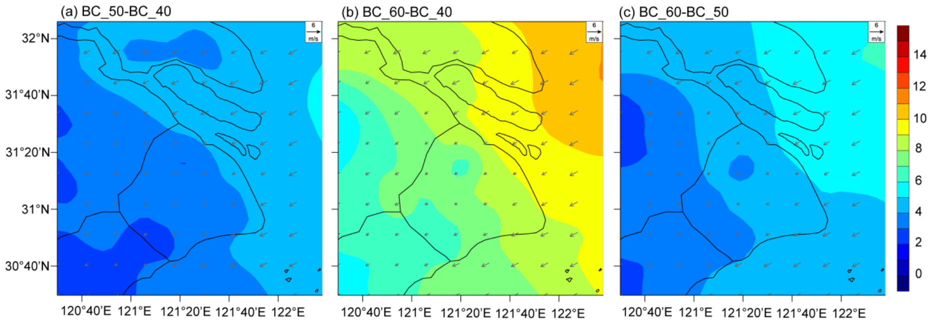

Figure 9 Mean differences in surface O_3 concentrations (ppbv) simulated with different chemical boundaries: (a) BC_50 minus BC_40, (b) BC_60 minus BC_40, and (c) BC_60 minus BC_50 in September 2014. Also shown is the calculated wind field (m s^{-1}) averaged over the simulation period.